Reconfigurable THz Filters Using Phase-Change Material and Integrated Heater

Varittha Sanphuang, *Student Member, IEEE*, Nima Ghalichechian, Niru K. Nahar, *Senior Member, IEEE*, and John L. Volakis, *Fellow, IEEE*

***Abstract*—We report the design, fabrication, and measurements of reconfigurable terahertz (THz) filters using vanadium dioxide (VO_2) phase-change material (PCM), which undergoes a transition between an insulator and metal phase at 68 °C (∼341 K). The filters are made of frequency selective surfaces (FSS) and heater are integrated for VO_2 excitation. Two THz spatial filters are developed. A broadband on/off filter at 0.35 THz is demonstrated with 20 dB change in transmission between the on and off states. Then, a reconfigurable stopband FSS filter with tunable rejection from 0.75 to 0.55 THz is presented. The latter shows a peak with rejection of more than 90%. The two states of both filters are achieved at relatively low temperature of 68 °C, making them suitable for practical applications. Comparisons between simulation and measurement show excellent agreement for both 0.35 THz on/off filter and 0.75 to 0.55 THz tunable filters.**

***Index Terms*—Periodic structures, phase-change materials (PCMs), reconfigurable, terahertz (THz) filter, vanadium dioxide (VO_2).**

I. Introduction

TERAHERTZ (THz) bands are of interest due to their unique applications in imaging and sensing, material characterization, space sciences, and short-range communications [1]–[8]. However, lack of fabricable components in this frequency range remains a challenge. Specifically, tunable filters are highly desired with reconfiguration. These filters are used to improve signal-to-noise ratio, block unwanted surrounding power, and allow for better detection of the desired field.

In this paper, we consider phase-change materials (PCMs) as a switching mechanism for the reconfigurable frequency selective surfaces (FSS) filter. PCMs refer to materials that exhibit the transition from dielectrics to conductors driven by external excitations, such as heat, electric field, optically injected charges, external stress or pressure [9], [10]. Various PCMs have been considered [9]–[13], corresponding to a wide range of transition temperatures. However, most of these PCMs [12] have their transition temperatures significantly below room temperature, implying that a cooling system is needed for triggering the switch. For all practical purposes, we require PCMs where a heater is employed.

Manuscript received October 28, 2015; revised March 14, 2016; accepted April 15, 2016. Date of publication May 18, 2016; date of current version July 08, 2016.

The authors are with the ElectroScience Laboratory, Department of Electrical and Computer Engineering, The Ohio State University, Columbus, OH 43212 USA (e-mail: sanphuang.1@osu.edu; ghalichechian.1@osu.edu; nahar.2@osu.edu; volakis.1@osu.edu).

Color versions of one or more of the figures in this paper are available online at http://ieeexplore.ieee.org.

Digital Object Identifier 10.1109/TTHZ.2016.2560175

Among various PCMs, vanadium dioxide (VO_2) is one such material that undergoes a transition between an insulator and metal phases at 68 °C (∼341 K), which is closest to room temperature. Importantly, PCM can be easily integrated into microsystems. The latter property makes VO_2 PCMs attractive for reconfigurable filters [14], [15]. Though there are several studies of the reconfigurable applications using PCM [14]–[26], none of them employs build-in temperature control [15]. In this paper, an integrated heater is introduced to enable thermal excitation of VO_2 in a practical manner. Reconfiguration is also demonstrated achieving tunability for THz FSS filters with the integrated heater. This controlled heater enhances the practical realization of this type of filters.

In this paper, two types of THz spatial filters are examined: 1) a broadband on/off filter; and 2) a frequency reconfigurable stopband filter. The integrated heater is designed to control the filter temperature without affecting the performance of the filter. The VO_2 thin-film process development is extensively discussed and measurements are provided that verify the VO_2 performance in both states.

II. Designs

Several high-performance THz filters are commercially available. However, their frequency response is fixed and do not provide a tunable frequency selectivity. There is also interest in achieving controllable bandpass and bandstop filter characteristics. FSS, which are periodic, planar, and generally consist of metallic elements on dielectric layers, is considered here as a THz filter since it shows bandpass or bandstop characteristic based on its geometry [8], [27]–[31]. To achieve the reconfiguration, VO_2 thin film is introduced within the FSS structure. The film can be deposited onto a substrate or inserted as part of the structure. The challenge is to minimize losses and optimize overall filter performance by sharpening the roll-off response curves of the FSS filter.

Here, we discuss two designs for reconfigurable THz filter by using VO_2 thin film to:

1) reconfigure THz filters as ON/OFF filter at specific center frequency;
2) reconfigure THz filters as frequency shifting stopband filter.

A. Broadband ON/OFF Filter Design

Since the element type (geometry), substrates, superstrate, and interelement spacing play a significant role in the FSS's performance, the filter unit cell was carefully optimized. To

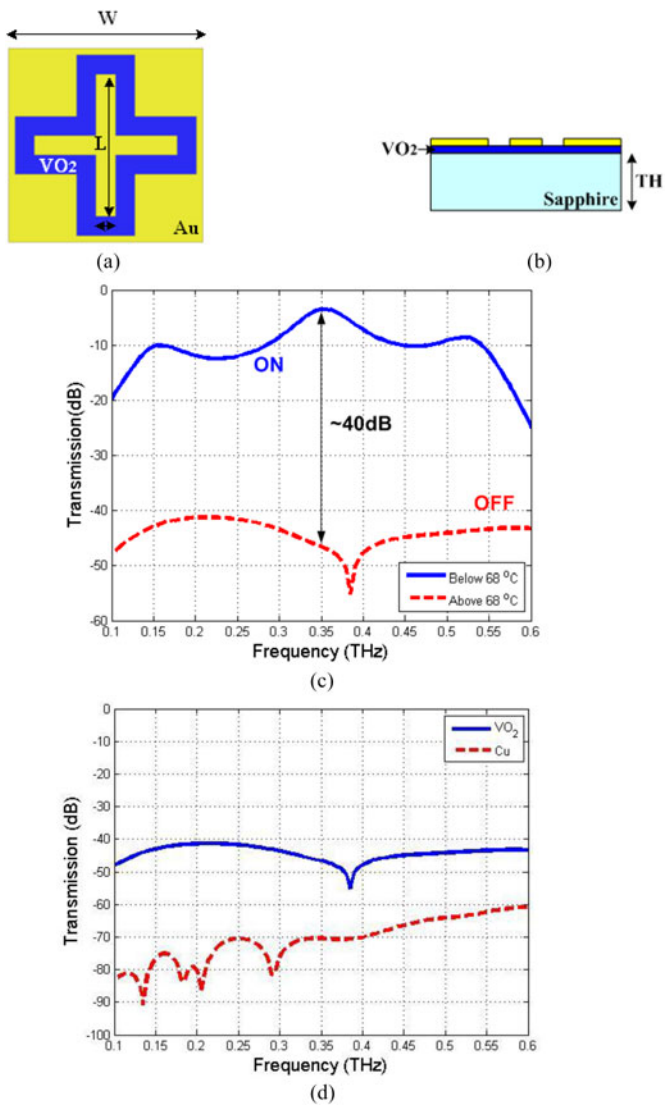

Fig. 1. Unit cell geometry of the proposed on/off FSS filter operating at THz frequencies. (a) Top view. (b) Side view. (c) Simulated transmission response. (d) Comparison of VO_2 to Cu at off stage.

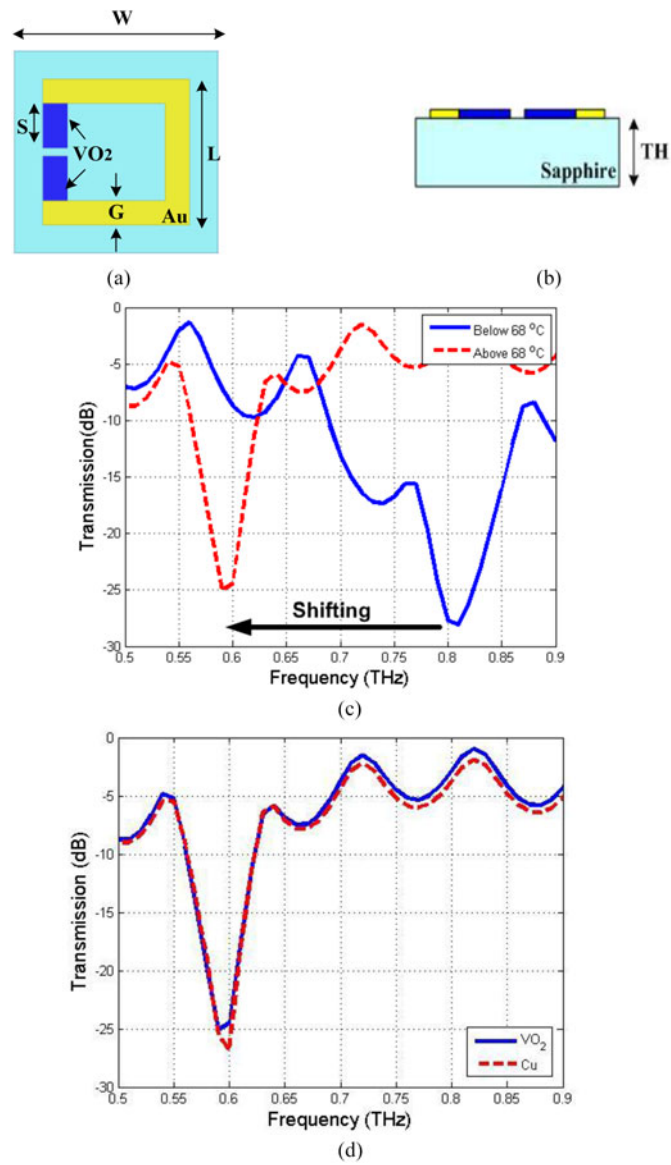

Fig. 2. Unit cell geometry of the proposed frequency shifting FSS filter operating at THz frequencies. (a) Top view. (b) Side view. (c) Simulated transmission response. (d) Comparison of VO_2 to Cu at conductor phase.

allow for sufficient design flexibility, a cross-loop FSS is chosen (shown in Fig. 1). For reconfiguration, VO_2 film is placed between the substrate and metal patterns as depicted in Fig. 1(b).

The geometry of the unit cell is illustrated in Fig. 1(a) and its dimensions were optimized using the full-wave simulation (Ansys HFSS). The frequency of interest for this design is 0.35 THz that lies in the low absorption atmospheric window with large available bandwidth [32]. The dimensions of this design are: unit cell size $W = 150\ \mu\text{m}$, cross length $L = 140\ \mu\text{m}$, and cross width $G = 15\ \mu\text{m}$. Also, the substrate is a *c*-plane sapphire of thickness $(TH) = 150\ \mu\text{m}$. The goal is to exploit the conductivity change of the VO_2 film from dielectric to conducting state as a function of temperature. Specifically at above ~68 °C, the VO_2 film becomes metallic and blocks the incoming wave. Therefore, the filter acts as a reflector (off state). This filter has two states (on/off) when the temperature is below/above ~68 °C. As shown in Fig. 1(a), 40 dB difference is achieved at 0.35 THz. Full-wave simulations [see Fig. 1(c)] demonstrate the concept. In Fig. 1(d), we have also compared the ohmic losses of VO_2 in the conductor phase to Cu (conductivity $= 5.8 \times 10^7$ S/m) as the standard material. There is ~30 dB difference in transmission at off stage between VO_2 and Cu as expected due to lower conductivity of VO_2.

B. Frequency Reconfigurable Stopband Design

As the second design, we considered a reconfigurable THz filter using a combination of VO_2 thin film and gold to form the FSS structure (hybrid design). The unit cell is depicted in Fig. 2 as a square loop with a gap at the left. One side of the square FSS unit cell is constructed of VO_2 films and serves to alter the filter's response when the VO_2 transitions through its

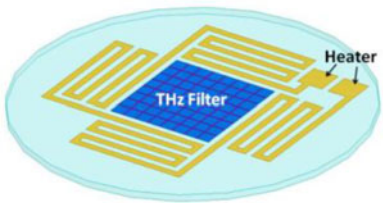

Fig. 3. Meander loop heater around the THz filter.

phases. The FSS was designed to operate between 0.5 to 0.9 THz. We note that the 0.6 and 0.8 THz frequency were chosen which are typical for THz security imagers used in atmospheric windows [33]. The dimension of the unit cell are: unit cell size $W = 50\ \mu\text{m}$, C-shape length $L = 36\ \mu\text{m}$, C-shape width $G = 6\ \mu\text{m}$ with the VO_2 leg of $10\ \mu\text{m} \times 6\ \mu\text{m}$. Again *c*-plane sapphire of thickness $(TH) = 430\ \mu\text{m}$ was used as a substrate.

The design in Fig. 2 achieved a stopband rejection that shifted from 0.8 to 0.6 THz when the VO_2 reached its metallic state (temperature $>$ 68 °C). The filter is suitable for cases when large frequency shifting is required. Again, we compared the ohmic losses of VO_2 in conductor phase to Cu. There is a very small difference in transmission ($\sim$2 dB) at the same frequency peak. As it can be seen from Figs. 1(a) and 2(a), the on/off filter structure has more metallization compared to the frequency shifting filter. Thus, the higher metallization causes lesser ohmic loss due to change in materials in unit cells.

C. Integrated Controlled Heater Design

Microheaters are well known in various microelectromechanical (MEMS) devices and microfluidic applications to provide several functionalities, i.e., physical and chemical sensors, pumping and chemical reactor [34]–[36]. In most of these designs, the heater is placed underneath the structure. However, for our unique application of the heater in spatial filters, it cannot be placed underneath for performance purpose. To actuate through the VO_2 state, a heater is introduced at the periphery of the FSS filter instead of underneath as shown in Fig. 3 [15].

The heater functions as resistive heating, which is the process where the input energy from electric current is converted into heat through resistive losses in the material. In designing the heater, it is important to have low power consumption, low thermal mass, fast transition, and temperature uniformity across where the device is operated. In our application, the temperature uniformity across the VO_2 in every unit cell is the most significant feature since we want to ensure that every unit cell in the array get activated at the same time.

To do so, different geometries of heater are studied: circular, square, and meander designs, were considered as shown in Fig 4. Multiphysics simulation tool (COMSOL) was used to study heater topologies. Gold was deposited to form the heater circuit with identical thickness as of the FSS pattern. This simplified fabrication process was chosen since the same step can be used for patterning the FSS structure. Again, 2″ diameter *c*-plane sapphire is used as the substrate. For heat control, different voltages were applied× to achieve uniform temperature across the

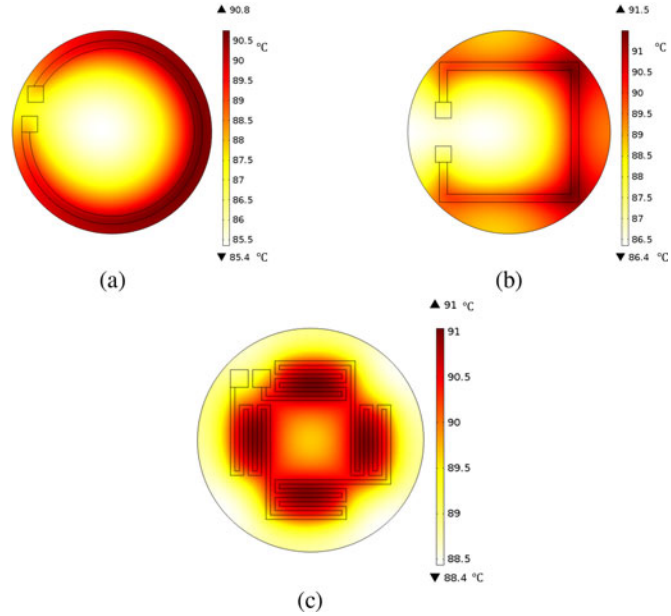

Fig. 4. Temperature contour of integrated heater surface with (a) circular, (b) square, and (c) meander designs.

$0.8'' \times 0.8''$ center area of the design. We found that to achieve temperature of 85 to 91°C, the applied voltages of 2.1, 2.05, and 5 V are required for each heater design, respectively. As shown in Fig. 4, the circular and square heater designs are simpler and require lower voltage. However, the meander heater design provides more uniform temperature at the center since the geometry of the design is symmetric. This structure reduces the device area and help confining the heat at the center. Furthermore, the power consumption of each design is studied. The resistance of heater circuit of circular, square, and meander designs are 3.01, 2.93, and 18.45 Ω, respectively. Based on the applied voltage mentioned above, the power consumption of each heater design is calculated and obtained as 1.47, 1.44, and 1.35 W. As seen, the meander design provides lower power consumption even though it requires higher voltage. This is due to that the meander design reduces the overall device area with higher resistance of the heater compared to the other two designs. Hence, it was adopted for reconfiguration of our device.

III. Fabrication

A. VO_2 Thin-Film Development

Before fabricating the FSS filter, high quality VO_2 thin film must be developed. Various VO_2 thin-film deposition techniques have been previously reported. They include pulsed laser deposition [37], sol-gel [38], RF reactive magnetron sputtering [39], and dc reactive magnetron sputtering [40]. For this paper, we employed dc reactive magnetron sputtering (AJA Orion) for VO_2 deposition. This approach provides conformal and uniform films on large sample area in a relatively low-cost batch process.

1) Deposition Process and Parametric Studies: The dc reactive magnetron sputtering with 99.5% Vanadium (V) target

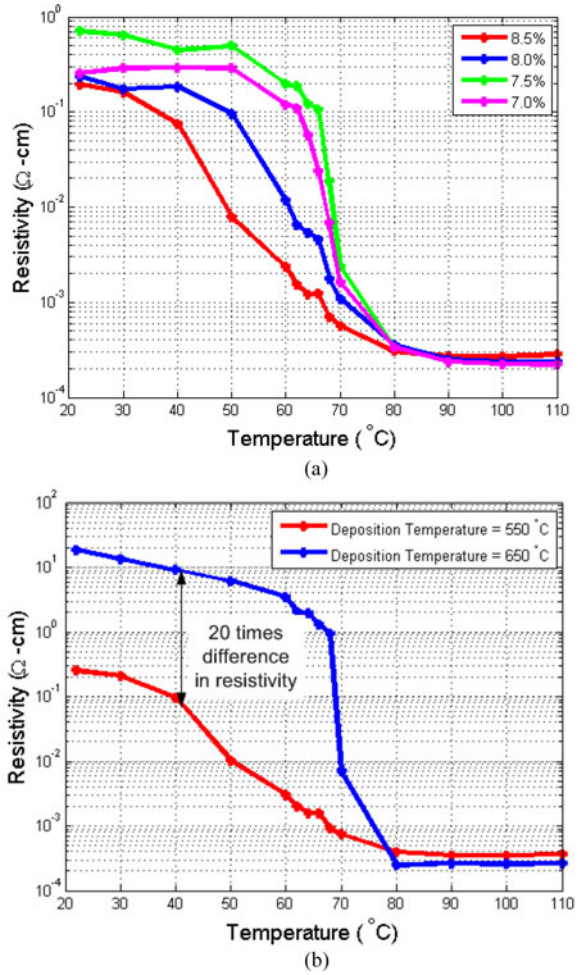

Fig. 5. (a) Resistivity versus excitation temperature for different Ar/O_2 injection ratio. (b) Resistivity versus excitation temperature for two deposition temperatures at 550 and 650 °C.

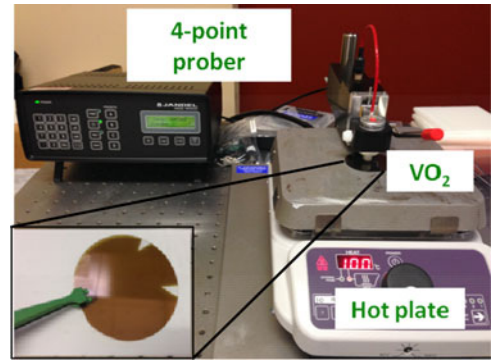

Fig. 6. Measurement setup (Inset: an example of VO_2 thin film deposited on a sapphire substrate) [20].

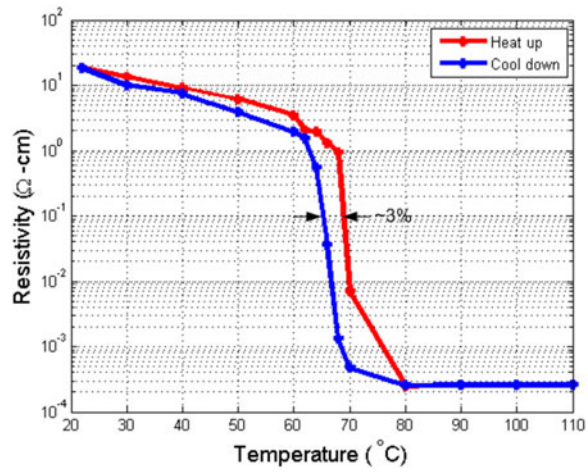

Fig. 7. Hysteresis loop of our developed VO_2 sample.

is used to deposit on 2″ *c*-plane (0001) sapphire substrate. In this system, argon (Ar) is used as a carrier and oxygen (O_2) is injected as reactive gas to create the oxide. There are several critical parameters in depositing VO_2. Among them are: power, pressure, Ar/O_2 gas injection ratio, and deposition temperature.

Several attempts were made to achieve successful growth conditions. The Ar/O_2 injection ratio was studied and shown in Fig. 5(a) by varying the percentage of O_2 from 7% to 8.5%. It was observed that there is a small window for optimizing the resistivity ratio (i.e., ratio of resistivity below and above transition temperature). The deposition was performed at various temperatures ranging from 500 to 650 °C. As shown in Fig. 5(b), the deposition temperature impacts the resistivity ratio of the VO_2 film. Specifically, deposition at 650 °C provides about 20 times higher resistivity compared to 550 °C. This is important as we require as large as possible resistivity change. Finally, we have tuned the electrical and phase transition properties of our film to achieve largest conductivity change at ∼68 °C. The VO_2 thin films have been grown with Ar/O_2 gas flow of 92.5/7.5 sccm. The deposition temperature is set to be 650 °C and the base pressure before sputtering is controlled to be below 10^{-6} Torr. The pressure is kept constant at 10 mTorr throughout the deposition. The final VO_2 film thickness is measured to be 80 nm for all design work.

2) Resistivity Measurement Setup: For measurement setup, the film is positioned on a hot plate and measurements are carried out as the temperature is varied in 2–10 °C steps. The overall resistivity measurement setup is shown in Fig. 6. A four-point probe (Jandel RM3000) was used to measure the sheet resistance of the film at dc. Then, the thickness of the film was measured using a Dektek profilometer. Finally, the resistivity of VO_2 versus temperature is determined from sheet resistance and thickness measurements.

3) Optimized VO_2 *Thin-Film Resistivity:* The resistivity ratio of our optimized VO_2 film is 7×10^4 times. This difference is observed as the temperature changes from 60 to 80 °C. As depicted in Fig. 7, our film shows low hysteresis of 3% during the heat up and cools down stages. The measured conductivity (σ) of our film at the two different temperatures is $\sigma = 5.38\ \mathrm{S/m}$ (dielectric phase) and $\sigma = 3.77 \times 10^5$ S/m (conductor phase), respectively.

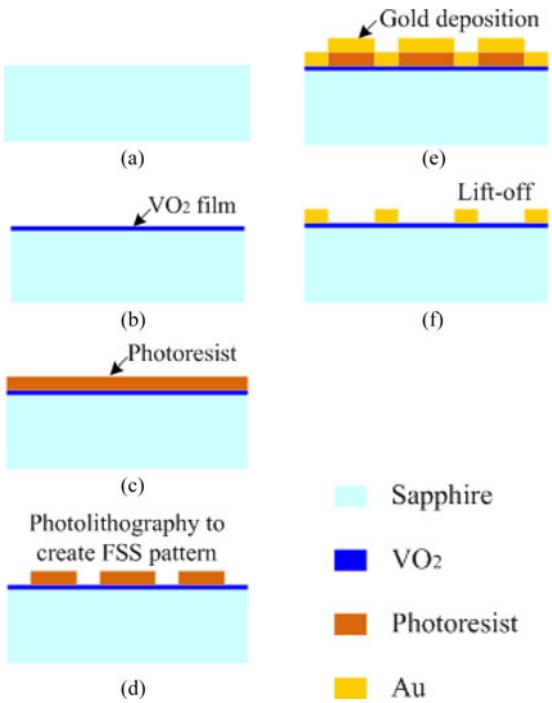

Fig. 8. Steps used to fabricate the broadband THz filter: (a) sapphire substrate, (b) VO_2 sputtering deposition, (c) photoresist spinning, (d) photolithography, (e) Au deposition, and (f) lift-off.

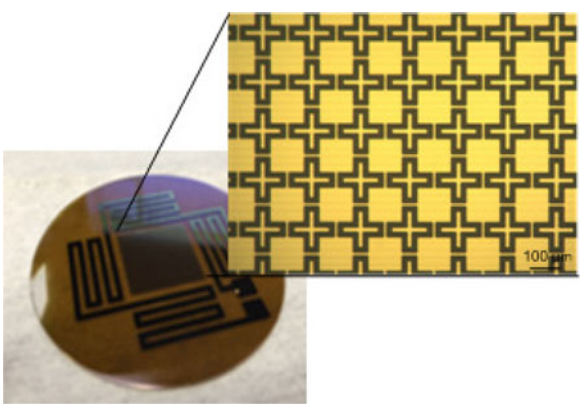

Fig. 9. Fabricated broadband on/off FSS filter with heater surrounding the FSS (inset: microscopic image).

B. Filters Fabrication

Upon achieving a high quality VO_2 thin-film deposition with 710^4 change in resistivity, we proceeded to realize two reconfigurable THz filters on a *c*-plane sapphire substrate. Standard photolithography, thin-film deposition, and lift-off techniques were used for fabricating on/off filter. The process is illustrated in Fig. 8. The final fabricated structure is shown in Fig. 9. First, the VO_2 thin film (80 nm thick) is deposited using dc sputtering as mentioned in the previous section. Next the standard photolithography step with image-reversal AZ5214E photoresist is used to pattern the periodic structure and heater. Then, a 200-nm thick gold (Au) layer is deposited using e-beam evaporator

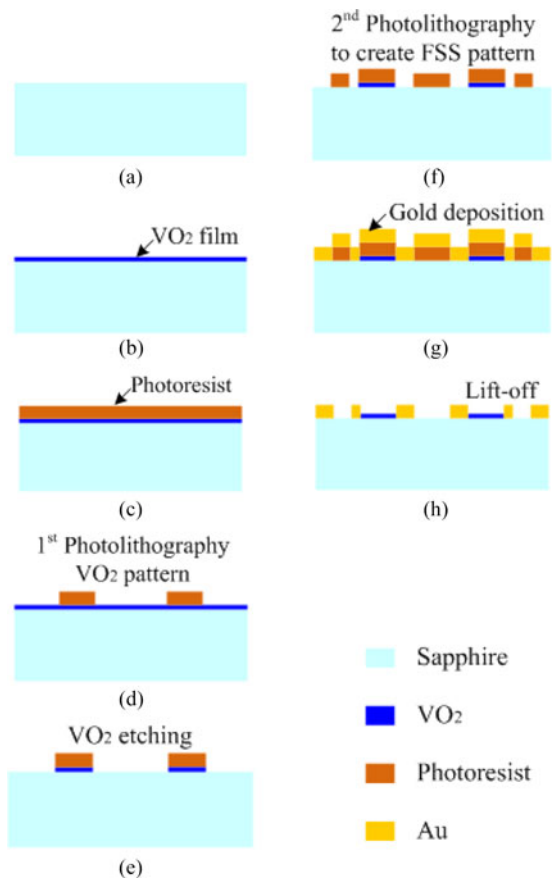

Fig. 10. Steps used to fabricate the frequency reconfigurable stopband THz filter: (a) sapphire substrate, (b) VO_2 sputtering deposition, (c) photoresist spinning, (d) first photolithography for pattering VO_2 legs, (e) VO_2 etching, (f) second photolithography to define FSS filter and heater structure, (g) Au deposition, and (h) lift-off process.

(CHA Solution) followed by a lift-off step to achieve the final structures.

Unlike the previous device, the frequency shifting stopband filter requires patterned VO_2 film instead of a blank thin film. Therefore, the following steps are followed: after the VO_2 deposition, the film is patterned using photolithography by S1813 positive photoresist. VO_2 film is then etched for 5 min in hydrogen peroxide (30% by weight) solution. After photoresist removal, a second lithography step is performed using image-reversal AZ5214E photoresist. This step gives the patterned VO_2 as depicted in Fig. 10. Then the 200-nm thick gold layer is deposited using e-beam evaporator. Finally, the pattern is achieved by a lift-off step (see Fig. 10). The frequency reconfigurable stopband filter is fabricated and shown in Fig. 11.

IV. Measurements and Validation

The transmission of the fabricated THz filters was measured using a time-domain spectroscopy (TPS 3000 system, Teraview, Ltd.) at normal incidence $(\theta = 0^\circ)$. The schematics of the THz time-domain spectrometer (THz-TDS) in transmission mode is illustrated in Fig. 12(a) [8]. Using this setup, the broadband THz pulses were generated for the FSS filter excitation using a

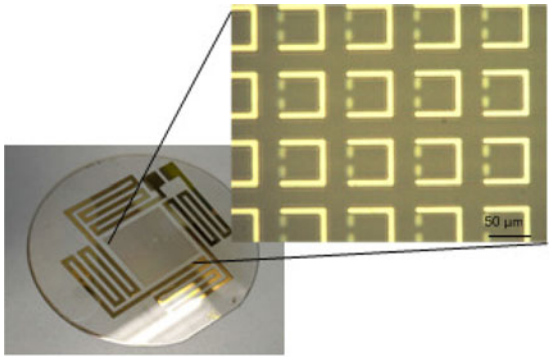

Fig. 11. Fabricated frequency reconfigurable stopband filter with heater surrounding the FSS (inset: microscopic image).

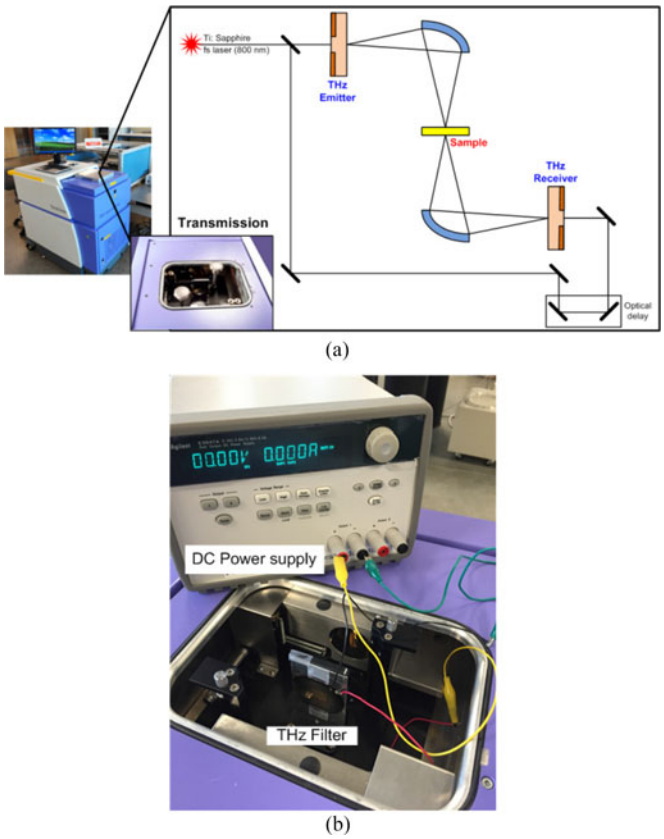

Fig. 12. (a) Schematics of THz time-domain spectrometer in transmission mode and (b) measurement setup.

photoconductive antenna. This antenna was excited via a pulsed near-infrared laser, which covers a frequency range of 0.06–3 THz. The incident THz excitation from the photoconductive antenna is focused through a curved reflector before incidence on the FSS sample. Transmission through the sample is then measured using the THz-TDS transmission gantry. During the process, voltage is applied to the heater with the range of 0–20 V. Power to the heater is controlled by varying the voltage to achieve two phases of VO_2. An aluminum sample holder is also used to help dissipating the heat. The overall measurement setup is shown in Fig. 12(b). The heater reached 70 °C after 18 V is

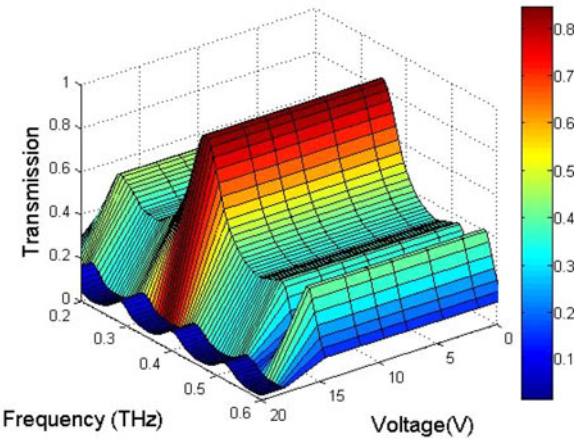

Fig. 13. Transmission of broadband on/off filter versus frequency (0.2–0.6 THz) for different voltages applied to the heater.

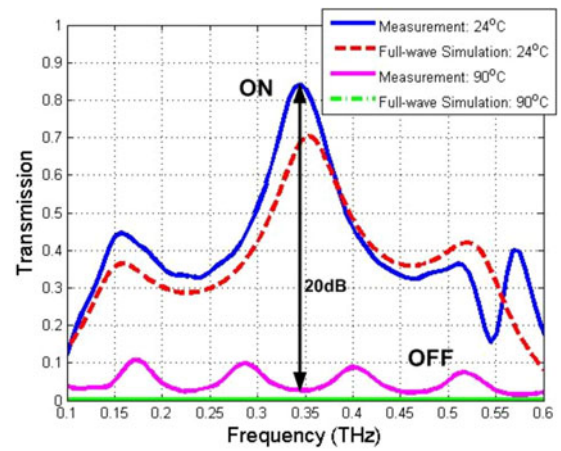

Fig. 14. Comparison of simulated and measured transmission response of the broadband on/off THz filter.

applied within 30 s and cooled down to room temperature within 45 s with the help of aluminum sample holder.

A. Broadband ON/OFF Filter Measurement

The transmission response of the filter in Fig. 9 is plotted in Fig. 13. This three-dimensional response gives the transmission itself as a function of applied voltage to the heater and the frequency of the excitation signal. It is shown that the transmission peak is at 0.35 THz [at room temperature (24 °C)] and drops nearly to 0.1 when voltage reaches 18 V at 70 °C.

Fig. 14 compares the measured and simulated (as in Fig. 1) curves of the transmission response for the broadband on/off THz filter. The agreement between the two curves is good but most important, the on and off behaving of the filter as the VO_2 temperature is at 24 and 90 °C is quite clear. The frequency range of interest is from 0.1 to 0.6 THz. We note that the transmission peak shows high% of transmission (∼83%) at 0.35 THz. At 90 °C, there is some difference between measurement and simulation results. This is most likely due to ideal conductivity

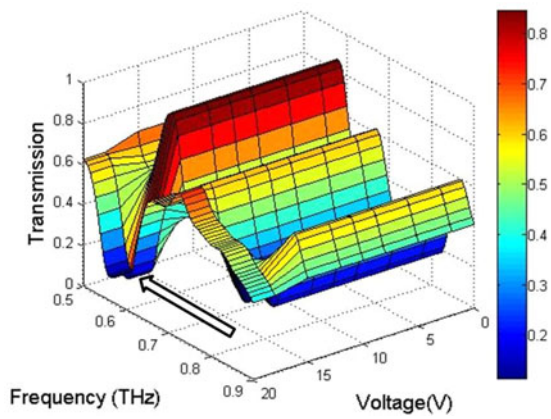

Fig. 15. Transmission of frequency shifted stopband filter versus frequency (0.5–0.9 THz) for different voltages applied to the heater.

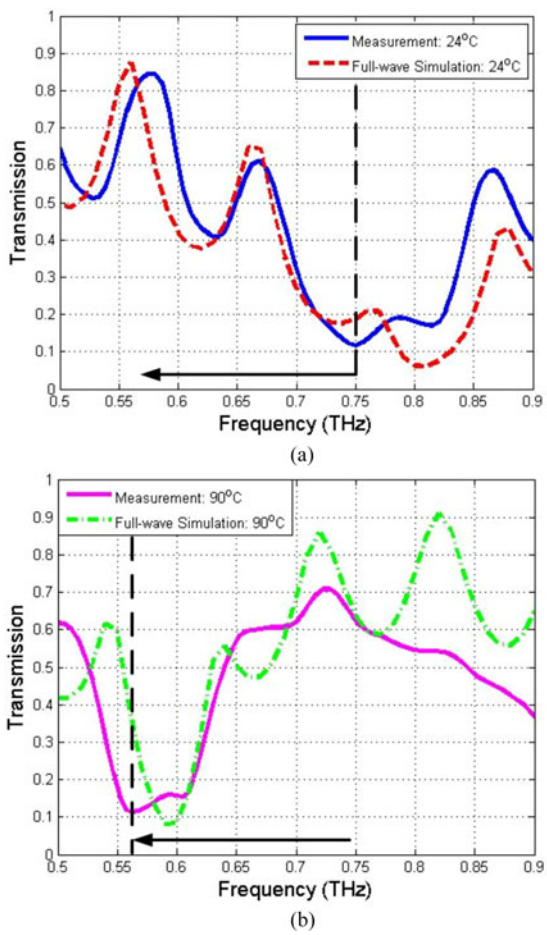

Fig. 16. Comparison of simulated and measured transmission response of the frequency reconfigurable stopband THz filter at (a) 24 °C and (b) 90 °C.

used in the simulation and the actual material used in fabrication. In addition, the Fabry–Perot effect taking place within the sapphire substrate could lower the filter performance. As the temperature increases beyond the transition point (68 °C), the transmission peak vanishes and overall transmission drops by 20 dB. This shows the performance of switch on and switch off functionality of the filter at 0.35 THz. Please note that the off state of this filter can be explained by a Fabry–Perot effect in the sapphire substrate. In order to avoid the evanescent waves to propagate through FSS structure, the thickness of the dielectric substrate should be less than the wavelength $\lambda/20$ [27]. However, due to the lack of availability of thinner sapphire substrate, 150-μm thick sapphire was used.

B. Frequency Reconfigurable Filter Measurement

The transmission responses of the reconfigurable stopband filter as a function of the applied voltage to the heater is plotted in Fig. 15. It is observed that the stopband is shifted downward from 0.75 to 0.55 THz at 18 V. Fig. 16(a) shows the comparison between measurement and simulation (as in Fig. 2) at 24 °C. There is a small shift from 0.8 to 0.75 THz and the bandwidth is broader. At 90 °C, the stopband peak is shifted to 0.55 from 0.6 THz. This difference between the measured and simulation results can be attributed to the minor misalignment during the fabrication processes and the undercut while etching the VO_2 patterns. However, the measured responses still shows a large shift ($\sim$0.2 THz) as the temperature increases above the transition temperature. This design can be considered as an experimental demonstration for the frequency reconfigurable stopband THz filter in the range of 0.5–0.9 THz.

V. Conclusion and Future Work

We developed and measured the reconfigurable THz filters using FSS and PCM: VO_2 integrated with heater. The goal was for an excellent transmission of THz filter with reconfigurable properties to improve THz applications' selectivity. Two designs are achieved here as broadband on/off THz filter and frequency reconfigurable stopband THz filter. For on/off filter, the VO_2 thin film is deposited between FSS pattern and substrate. The peak frequency of this reconfigurable THz filter is at 0.35 THz and the peak is suppressed when the temperature increases beyond the transition temperature (68 °C). For stopband filter, the VO_2 thin film is patterned as part of the FSS structure. There is a shift of frequency from 0.75 down to 0.55 THz as temperature increased above 68 °C. Further, the integrated heater is first introduced here to provide practical realization for reconfigured filter with high performance. Such filters are great candidates for next-generation THz sensing, spectroscopy, and imaging applications. Although only a specified range of frequency and only VO_2 were considered here, improved filter designs with different design geometries, other selected materials, and substrates could allow for different frequency ranges and higher filter performances. In addition, the heater can be further optimized to provide faster speed and better temperature control.

References

[1] P. H. Siegel, "Terahertz technology," *IEEE Trans. Microw. Theory Techn.*, vol. 50, no. 3, pp. 910–928, Mar. 2002.
[2] A. Redo-Sanchez and X.-C. Zhang, "Terahertz science and technology trends," *IEEE J. Sel. Topics Quantum Electron.*, vol. 14, no. 2, pp. 260–269, Mar./Apr. 2008.
[3] M. C. Kemp *et al.*, "Security applications of terahertz technology," *Proc. SPIE*, vol. 5070, pp. 44–52, Aug. 2003.

[4] T. Yeh *et al.*, "Ultra-broad and sharp-transition bandpass terahertz filters by hybridizing multiple resonances mode in monolithic metamaterials," *Opt. Express*, vol. 20, no. 7, pp. 7580–7589, Mar. 2012.

[5] T. Driscoll *et al.*, "Memory metamaterials," *Science*, vol. 325, pp. 1518–1521, Sep. 2009.

[6] V. Sanphuang, N. K. Nahar, and J. L. Volakis, "Broadband THz filters for THz sensing devices," in *Proc. IEEE Nat. Aerosp. Electron. Conf.*, Jul. 2012, pp. 18–19.

[7] M. C. Kemp *et al.*, "Security applications of terahertz technology," *Proc. SPIE*, vol. 5070, pp. 44–52, 2003.

[8] V. Sanphuang, W.-G. Yeo, J. L. Volakis, and N. K. Nahar, "THz transparent metamaterials for enhanced spectroscopic and imaging measurements," *IEEE Trans. THz Sci. Technol.*, vol. 5, no. 1, pp. 117–123, Jan. 2015.

[9] N. F. Mott, *Metal-Insulator Transitions*. London, U.K.: Taylor & Francis, 1990, p. 286.

[10] M. Imada, A. Fujimori, and Y. Tokura, "Metal-insulator transitions," *Rev. Mod. Phys.*, vol. 70, pp. 1039–263, 1998.

[11] A. Adler, "Mechanisms for metal-nonmetal transitions in transition-metal in oxides and sulfides," *Rev. Mod. Phys.*, vol. 40, pp. 714–736, 1968.

[12] Z. Yang, C. Ko, and S. Ramanathan, "Oxide electronics utilizing ultrafast metal-insulator transitions," *Annu. Rev. Mater. Res.*, vol. 41, pp. 337–367, Aug. 2011.

[13] G. Stefanovich, A. Pergament, and D. Stefanovich, "Electrical switching and Mott transition in VO_2," *J. Phys. Condens. Matter*, vol. 12, pp. 8837–8845, 2000.

[14] V. Sanphuang, N. Ghalichechian, N. K. Nahar, and J. L. Volakis, "Phase change materials for reconfigurable systems," presented at the IEEE AP-S/URSI Radio Science Meeting, Memphis, TN, USA, 2014.

[15] V. Sanphuang, N. Ghalichechian, N. K. Nahar, and J. L. Volakis, "Reconfigurable THz filters with integrated micro-heater," presented at the IEEE Antennas Propagation Society Int. Symp., Memphis, TN, USA, 2014.

[16] B.-J. Kim *et al.*, "Temperature dependence of the first-order metal-insulator transition in VO_2 and programmable critical temperature sensor," *App. Phys. Letts.*, vol. 90, 2007, Art. no. 023515.

[17] H. N. S. Krishnamoorthy, Y. Zhou, S. Ramanathan, E. Narimanov, and V. M. Menon, "Tunable hyperbolic metamaterials utilizing phase change heterostructures," *App. Phys. Letts.*, vol. 104, 2014, Art. no. 121101.

[18] H. T. Chen *et al.*, "Electromagnetic metamaterials for terahertz applications," *IEEE Trans. THz Sci. Technol.*, vol. 1, no. 1, pp. 42–50, Mar. 2008.

[19] A. Crunteanu *et al.*, "Tunable terhertz metamaterials based on metal-insulator phase transition of VO_2 layers," presented at the IEEE MTT-S Int. Microwave Symp. Dig., Montreal, QC, Canada, Jun. 2012.

[20] V. Sanphuang, N. Ghalichechian, N. K. Nahar, and J. L. Volakis, "Bandwidth reconfigurable THz filter employing phase-change material," in *Proc. IEEE APS/URSI Int. Symp. Antennas Propag.*, Vancouver, BC, Canada, 2015, pp. 565–566.

[21] Z. Yang, C. Ko, V. Balakrishnan, G. Gopalakrishnan, and S. Ramanatha, "Dielectric and carrier transport properties of vanadium dioxide thin films across the phase transition utilizing gated capacitor devices," *Phys. Rev. B*, vol. 82, 2010, Art. no. 205101.

[22] S. D. Ha, Y. Zhou, A. E. Duwel, D. W. White, and S. Ramanathan, "Quick switch: Strongly correlated electronic phase transition systems for cutting-edge microwave devices," *IEEE Microw. Mag.*, vol. 15, no. 6, pp. 32–44, Sep./Oct. 2014.

[23] M. J. Dicken1 *et al.*, "Frequency tunable near-infrared metamaterials based on VO_2 phase transition," *Opt. Express*, vol. 17, pp. 18330–18339, 2009.

[24] Y. Zhu *et al.*, "Tunable dual-band terahertz metamaterial bandpass filters," *Opt. Lett.*, vol. 38, no. 14, pp. 2382–2384, Jul. 2013.

[25] B.-J. Kim, Y.-W. Lee, S. Choi, B.-G. Chae, and H.-T. Kim, "Analysis of the surface morphology and the resistance of VO_2 thin films on M-plane Al_2O_3," *J. Korean Phys. Soc.*, vol. 50, no. 3, pp. 653–656, 2007.

[26] M. Seo *et al.*, "Active terahertz nanoantennas based on VO_2 phase transition," *Nano Lett.*, vol. 10, pp. 2064–2068, 2010.

[27] B. A. Munk, *Frequency Selective Surfaces, Theory and Design*. New York, NY, USA: Wiley-Interscience, 2000.

[28] R. Mittra, C. H. Chan, and T. Cwik, "Techniques for analyzing frequency selective surfaces—A review," *Proc. IEEE*, vol. 76, no. 12, pp. 1593–1615, Dec. 1988.

[29] Y. E. Erdemli, K. Sertel, R. A. Gilbert, D. E. Wright, and J. L. Volakis, "Frequency selective surfaces to enhance performance of broadband reconfigurable arrays," *IEEE Trans. Antennas Propag.*, vol. 50, no. 12, pp. 1716–1724, Dec. 2002.

[30] V. Sanphuang, N. K. Nahar, and J. L. Volakis, "Frequency selective surfaces filters to enhance performance of Ka band applications," *Microw. Opt. Technol. Lett.*, vol. 56, no. 3, pp. 563–568, Mar. 2014.

[31] V. Sanphuang, N. Ghalichechian, N. K. Nahar, and J. L. Volakis, "Equivalent circuit for VO_2 phase change material film in reconfigurable frequency selective surfaces," *App. Phys. Letts.*, vol. 107, 2015, Art. no. 253106.

[32] R. Piesiewicz *et al.*, "Short-range ultra-broadband terahertz communications: Concepts and perspectives," *IEEE Antennas Propag. Mag.*, vol. 49, no. 6, pp. 24–39, Dec. 2007.

[33] E. Bründermann, H.-W. Hübers, and M. F. Kimmitt, *Terahertz Techniques*. Berlin, Germany: Springer-Verlag, 2012.

[34] D. Briand *et al.*, "Micro-hotplates on polymide for sensors and actuators," *Sens. Actuator A, Phys.*, vol. 132, pp. 317–324, 2006.

[35] J. Yeom, C. R. Field, B. Bae, R. I. Masel, and M. A. Shannon, "The design, fabrication and characterization of a silicon microheater for an integrated MEMS gas preconcentrator," *J. Micromech.Microeng.*, vol. 18, 2008, Art. no. 125001.

[36] Q. Zhou *et al.*, "Fast response integrated MEMS microheaters for ultra low power gas detection," *Sens. Actuator A, Phys.*, vol. 223, pp. 67–75, 2015.

[37] J. Jian, A. Chen, W. Zhang, and H. Wang, "Sharp semiconductor-to-metal transition of VO_2 thin film on glass," *J. Appl. Phys.*, vol. 114, 2013, Art. no. 244301.

[38] T. J. Hanlon, R. E. Walker, J. A. Coath, and M. A. Richardson, "Comparison between vanadium dioxide coatings on glass produced by sputtering, alkoxide and aqueous sol-gel methods," *Thin Solid Films*, vol. 405, pp. 234–237, Feb. 2002.

[39] D. Ruzmetov, K. T. Zawilski, V. Narayanamurti, and S. Ramanathan, "Structure-functional property relationships in RF-sputtered vanadium dioxide thin film," *J. Appl. Phys.*, vol. 102, 2007, Art. no. 113715.

[40] Y. Zhao *et al.*, "Structural, electrical, and terahertz transmission properties of $\mathbf{VO_2}$ thin films grown on c-, r-, and m-plane sapphire substrates," *J. Appl. Phys.*, vol. 111, 2012, Art. no. 053533.

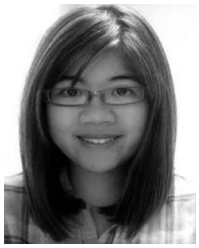

Varittha Sanphuang (S'09) was born in Bangkok, Thailand. She received the B.Eng. degree (first honor) in electrical and electronics engineering from Asian University, Chon Buri, Thailand, in 2010, and is currently working toward the Doctoral degree at The Ohio State University, Columbus, OH, USA.

She is a Graduate Research Associate at the ElectroScience Laboratory at The Ohio State University. Her research areas include IR filter, metamaterials, and reconfi-gurable devices in high frequency, especially in Ka band and THz regions and also microfabrication techniques for microdevices.

Ms. Sanphuang received the 2009 IEEE Antennas and Propagation Society Predoctoral Research Award and the 2009 IEEE Microwave Theory and Techniques Society Undergraduate/Pre-Graduate Scholarship.

Nima Ghalichechian (S'99–M'08–SM'14) received the Ph.D. degree in electrical engineering from the University of Maryland, College Park, MD, USA, in 2007. His Ph.D. dissertation was titled "Design, Fabrication, and Characterization of a Rotary Variable-Capacitance Micromotor Supported on Microball Bearings."

He was with the Research Department of FormFactor, Inc., Livermore, CA, USA, as a Senior Principal Engineer from 2007 to 2012. During this period, he helped to design and develop microsprings for advanced probe cards used in testing memory and SoC semiconductor devices. He joined the ElectroScience Laboratory of The Ohio State University (OSU), Columbus, OH, USA, as a Research Scientist in 2012 and is currently a Research Assistant Professor at the Department of Electrical and Computer Engineering. His research is interdisciplinary and centers around two areas of micro/nanotechnology and electromagnetics. Specifically, he conducts research on RF microsystems with focus on reconfigurable antenna arrays, millimeter-wave antennas, terahertz microsystems, sensors, novel materials, and microfabrication processes. As a principal investigator, he has helped establishing several new programs at OSU sponsored by NSF, DARPA, and AFRL.

Niru K. Nahar (S'04–M'08–SM'13) received the B.Sc. (Hons.) degree in physics from Dhaka University, Dhaka, Bangladesh, the M.S. degree in physics from the Indiana University of Pennsylvania, Indiana, PA, USA, and the M.S. and Ph.D. degrees in electrical and computer engineering from The Ohio State University, Columbus, OH, USA, in 2002 and 2008, respectively.

She is currently a Research Assistant Professor at the ElectroScience Laboratory of the Electrical and Computer Engineering Department, The Ohio State University. She has been a Researcher at the ElectroScience Laboratory since 2008. She is also the Operational Manager of the new HELIOS (THz and mm-Wave) Laboratory at OSU which was established with the 3M grant from Ohio Third Frontier. She has more than three years of research experience in Optometry and Vision Science. She has also worked as a Research Intern at the Surface Analysis Laboratory in the Chemical and Metallurgical Division of Osram Sylvania, Inc., Towanda, PA, USA. She has authored 1 book, 24 journal articles, and 70+ conference proceedings and abstracts. Her current research focuses on the designs and characterization of THz and mmW sensors, THz spectroscopy systems for biomedical imaging, mmW ultrawideband low-profile antennas and phased arrays for cognitive sensing, reconfigurable arrays, novel RF-EO sensors and materials, optical true time delay engines, optical and mmW beam steering, and frequency selective surfaces.

Dr. Nahar is a member of the IEEE Antennas and Propagation Society, IEEE Photonics (formerly Lasers and Electro-Optics) Society, and the Optical Society of America. She served as the Secretary/Treasurer, Vice Chairman and Chairman of the IEEE Joint AP/MTT Chapter Columbus Section from 2011 to 2014. In 2015, she received Lumley Research Award from the College of Engineering of OSU for her outstanding research.

John L. Volakis (S'77–M'82–SM'89–F'96) was born in May 13, 1956, in Chios, Greece, and immigrated to USA in 1973. He received the B.E. degree, *summa cum laude*, from Youngstown State University, Youngstown, OH, USA, in 1978, and the M.Sc. and Ph.D. degrees from The Ohio State University, Columbus, OH., USA, in 1978 and 1982, respectively.

He started his career at Rockwell International (1982–1984), now Boeing. In 1984, he was appointed as an Assistant Professor at The University of Michigan, Ann Arbor, MI, USA, becoming a full Professor in 1994. He also served as the Director of the Radiation Laboratory from 1998 to 2000. Since January 2003, he is the Roy and Lois Chope Chair Professor of Engineering at the Ohio State University, Columbus, OH, and also serves as the Director of the ElectroScience Laboratory. Over the years, he carried out research in antennas, wireless communications and propagation, computational methods, electromagnetic compatibility and interference, design optimization, RF materials, multiphysics engineering, millimeter waves, and terahertz and medical sensing. His publications include 8 books, 375 journal papers, nearly 700 conference papers, 26 book chapters, and 16 patents/patent disclosures. Among his coauthored books are: *Approximate Boundary Conditions in Electromagnetics* (IET, U.K., 1995); *Finite Element Methods for Electromagnetics* (Wiley, 1998); 4th edition *Antenna Engineering Handbook* (McGraw Hill, 2007); *Small Antennas* (McGraw Hill, 2010); and *Integral Equation Methods for Electromagnetics* (SciTech, 2011). He has graduated/mentored more than 80 doctoral students/postdocs with 34 of them receiving best paper awards at conferences.

Dr. Volakis service to professional societies include: 2004 President of the IEEE Antennas and Propagation Society (2004), the Chair of USNC/URSI Commission B (2015–2017), twice the general Chair of the IEEE Antennas and Propagation Symposium, IEEE APS Distinguished Lecturer, IEEE APS Fellows Committee Chair, IEEE Wide Fellows Committee Member and Associate Editor of several journals. He was listed by ISI among the top 250 most referenced authors (2004), and is a Fellow ACES. Among his awards are: The University of Michigan College of Engineering Research Excellence Award in 1993, Scott Award from The Ohio State University College of Engineering for Outstanding Academic Achievement in 2011, IEEE AP Society C.-T. Tai Teaching Excellence Award in 2011, IEEE Henning Mentoring Award in 2013, IEEE Antennas & Propagation Distinguished Achievement Award in 2014, and the Ohio State University Distinguished Scholar Award in 2016.